Please cite this paper as : T. Zhu, S. Olthof, Th. Pauporté, Titanium dioxide Surface Energy Levels Tuning by Self-Assembled Monolayers. Appl. Phys. Lett. 121 (2022) 141602. DOI: 10.1063/5.0107202

Titanium dioxide Surface Energy Levels Tuning by Self-Assembled Monolayers

T. Zhu,[a] S. Olthof,[b]* Th. Pauporté[a]*

[a] Chimie ParisTech, PSL University, CNRS, Institut de Recherche de Chimie Paris (IRCP), 11 rue P. et M. Curie, F-75005 Paris, France.

[b] University of Cologne, Department of Chemistry, Greinstrasse 4-6, 50939 Cologne, Germany.

*Authors to whom correspondence should be addressed: solthof@uni-koeln.de; thierry.pauporte@chimieparistech.psl.eu

Abstract

Tailoring the work function of functional layers in an optoelectronic device is an important means for performance improvement, as it results in changes in charge extraction or recombination. One way to proceed is to adsorb molecules with varying dipole moment strength and sign. In this communication, the surface of anatase TiO_2 is modified using different self-assembled monolayers (SAMs) (4-chlorobenzoic acid, 4-nitrobenzoic acid, 4-methoxybenzoic acid, and β-alanine) and the energetics at the interface is determined using a series of photoelectron spectroscopy techniques, namely ultraviolet photoelectron spectroscopy (UPS), X-ray photoelectron spectroscopy (XPS), and inverse photoemission spectroscopy (IPES). The observed changes in work function are correlated to the dipole moments of the respective acids, calculated by density functional theory. Finally, the relevance of this interfacial engineering for controlling the charge extraction from an optoelectronic device is illustrated.

Keywords : TiO_2; SAMs; Work function; Photoelectron spectroscopy techniques; UPS; XPS

Titanium dioxide (TiO_2) layers are widely employed in the fast-developing field of emerging optoelectronic devices [1–11]. Their surface can be modified through self-assembled monolayers (SAMs) for the improvement of the interface between the metal oxide and semiconductors, thereby increasing the performance of devices [1,2,4–9,11–15]. One example here is the employment of SAMs on TiO_2 in perovskite solar cells (PSCs).[7,13,15-21] In our previous work, we investigated various

SAMs based on benzoic acid derivatives, and were able to show that the chlorine terminated one causes a distortion in the perovskite lattice due to the terminal chlorine atom binding to the lead. It resulted in an improved structural continuity between the perovskite and the TiO_2 layers and then a higher PSC performance compared to the untreated solar cells. [13,21]

Beyond the structural changes at the interface, the dipole moment of the SAMs also play an important role by affecting the work function (*Wf*) [22,23] which is a key factor impacting the energy level alignment at the interface.[3,13] By tuning this parameter, the charge extraction or recombination at the contact can be controlled and the performance of optoelectronic devices are directly affected.[17,22,23]. For instance, Zuo and co-authors studied the effect of SAM modification of ZnO on the performance of PSCs. They could show that the reduced work function introduced by the SAMs enhanced the charge extraction and thereby increased the photocurrent in devices. In addition, the charge recombination at the interface was also reduced, which was ascribed to the passivation of trap states. [17] Lu and co-authors studied the effect of SAMs on a perovskite layer. They found that the modification of the perovskite surface with SAMs could change the interfacial dipole and band alignment and thereby facilitate charge-transfer. [22]

Acid based SAMs are also of great interest since they bind to the oxide surface by means of their acid functional groups [24-27] and present a rather good stability.[30,31] They are attached to TiO_2 by their carboxylate group in a bidendate bridging mode.[5,32,33] In the case of rutile TiO_2, both of their oxygen atoms bind an adjacent pair of surface 5-fold-coordinated Ti atoms.[32,33] Johansson et al. investigated changes in energy levels at the interface between TiO_2, a dipole molecule (benzoic acid or 4-nitrobenzoic acid), and a polymer. Using XPS, they observed that the relative binding energy positions of S2p core level (originating from the polymer layer on top) versus Ti2p scales with the dipole moment of the adsorbed molecules [3].

In our previous work, we used a series of benzoic acid derivative SAMs on TiO_2 to improve the performance of organic-based UV-photodetectors. [5] The investigated acids were three para-substituted benzoic acid derivatives: 4-chlorobenzoic acid (CBA), 4-methoxy benzoic acid (MBA), and 4-nitro benzoic acid (NBA) completed by the β-alanine amino acid (also called 3-aminopropanoic acid and noted ALA). We were able to confirm the formation of the monolayer on the surface and investigated the changes in open circuit voltage (V_{oc}) and short circuit current (J_{sc}) of the respective devices.

To further analyze and understand the underlying reasons for the changes in device performance, a specific study of these SAMs/TiO_2 interfaces has been conducted in this communication using three different photoelectron spectroscopy techniques. The electronic structures and energy band levels of these systems have been fully unveiled. Here, we find an excellent correlation between the experimentally measured changes in work function and the calculated dipole moments of the SAMs.

Furthermore, based on these data, we have been able to correlate the changes induced by the SAMs to the performance of our organic-inorganic UV-photodetectors.

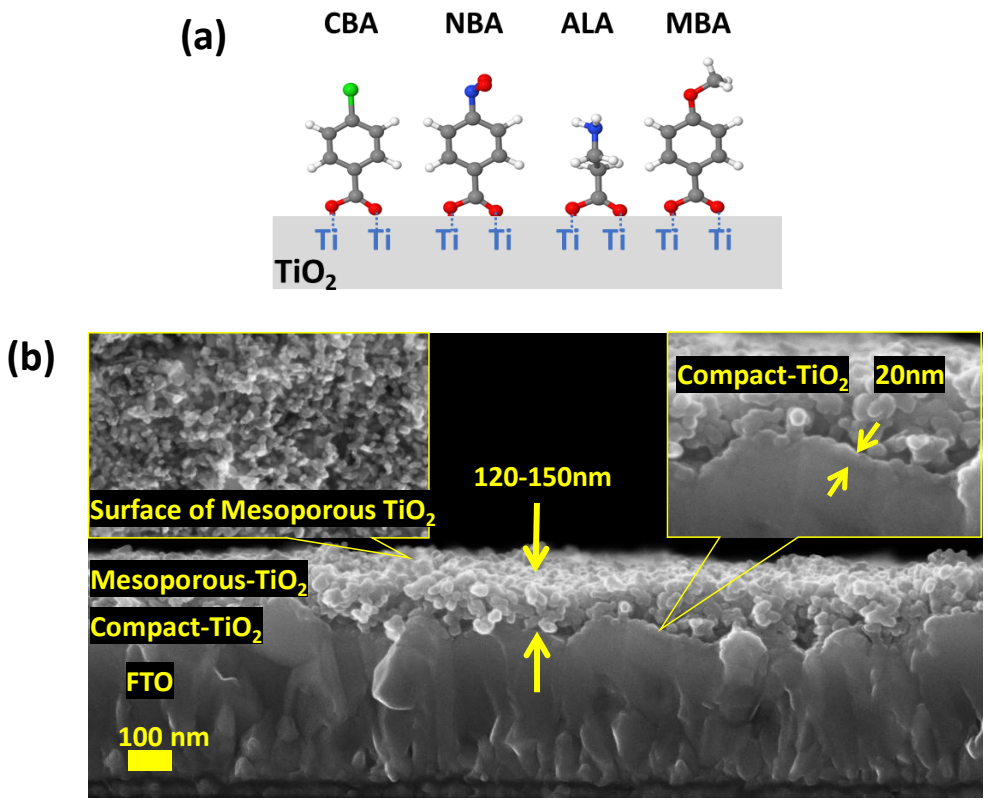

Figure 1: (a) Schematic molecular structure of the studied SAMs bonded to the anatase TiO_2 surface. From left to right: 4-chlorobenzoic acid, 4-nitro benzoic acid, β-alanine and 4-methoxy benzoic acid. White ball: hydrogen, grey: carbon, red: oxygen, blue: nitrogen and green: chlorine. (b) Cross-sectional SEM view of Glass/FTO/*c*-TiO_2/*meso*-TiO_2/SAMs. The left inset shows the morphology of *meso*-TiO_2 surface, and the right inset is a zoom view of the *c*-TiO_2 layer cross-section.

A scanning electron microscopy (SEM) cross-sectional view of the anatase TiO_2 mesoscopic substrate is presented in **Figure 1.** The sample consisted of a compact TiO_2 (*c*-TiO_2) layer deposited by spray pyrolysis on fluorine-doped tin oxide (FTO), topped by a mesoporous TiO_2 (*meso*-TiO_2) layer, deposited by spin-coating.[34,35] This structure underwent an annealing treatment at 500°C prior to be put in contact with the acids dissolved in solution to form the SAMs as described in the Experimental Section (Supporting Information). The investigated acids were : 4-chlorobenzoic acid (CBA), 4-methoxy benzoic acid (MBA), 4-nitro benzoic acid (NBA) and β-alanine (ALA) (**Figure 1a**). The thickness of the *c*-TiO_2 layer is estimated at 20 nm while the thickness of the *meso*-TiO_2 layer ranges between 120-150 nm. The diameter of the TiO_2 nanoparticles is around 30 nm. A top view image of the *meso*-TiO_2 surface is included as inset in **Figure 1b**. We checked that the TiO_2 morphology was not affected by the attachment of the SAM layers to the surface, as shown in the Supporting Information (**Figure S1)**. It should be noted that such *meso*-TiO_2 structures exhibit large surface areas and can therefore adsorb more dipolar SAM molecules compared to planar films.

Please cite this paper as : T. Zhu, S. Olthof, Th. Pauporté, Titanium dioxide Surface Energy Levels Tuning by Self-Assembled Monolayers. Appl. Phys. Lett. 121 (2022) 141602. DOI: 10.1063/5.0107202

The combination of various photoelectron spectroscopy techniques allowed us to fully characterize how the different SAMs affect the electronic structure of the mesoscopic TiO_2 surface. **Figure 2a** summarizes the UPS measurements of the pristine *meso*-TiO_2 and of the acid-modified surfaces. The left panel shows the high energy cutoff region from which the work function, *Wf*, was extracted ($Wf = h\nu$ (21.22 eV) – E_{cutoff}): the values are listed in **Table 1**. The cutoff region signal is dominated by the properties of the topmost layer and therefore shows how the SAMs modify the position of the vacuum level on the surface. On the other hand, the valence band region, in the right panel of **Figure 2a**, is rather dominated by the strong TiO_2 valence band feature starting at around 3.6 eV. To extract the signal originating from the SAMs, the spectra were modified by subtracting the pure meso-TiO_2 (black curve) from the SAM-covered measurements. For each data set, the intensity of the meso-TiO_2 signal for subtraction was adjusted to yield the best result, which was judged from the symmetry and Gaussian shape of the remaining SAM related density of states signal. The resulting curves are displayed in **Figure 2b**. Even though this procedure might introduce some errors, the spectra look very reasonable and can be used to extract the values for the hole injection barriers (E_{HOMO} *i.e.* the highest occupied molecular orbital (HOMO) onsets relative to E_F) which is then used to calculate the ionization energy (IE) values of the SAM molecules ($IE = E_{HOMO} + Wf$): the measured values are listed in **Table 1**. The analysis of TiO_2 was not only done by UPS, but also by using inverse photoelectron spectroscopy (IPES) which allowed us to determine the position of the conduction band (CB). The spectrum is shown in **Figure S2** (Supporting Information) and the extracted value of 0.15 eV above E_F is included in **Table 1**. IPES of the SAM-covered surfaces was not possible due to the comparably high noise level of the technique that makes it impossible to reliably detect the weak monolayer signals, so the position of the lowest unoccupied molecular orbital (LUMO) cannot be determined. As these SAM layers are very thin (here the thickness is lower than 1 nm), charge carriers should be able to tunnel through, so the LUMO positions will likely not affect the charge transport significantly.

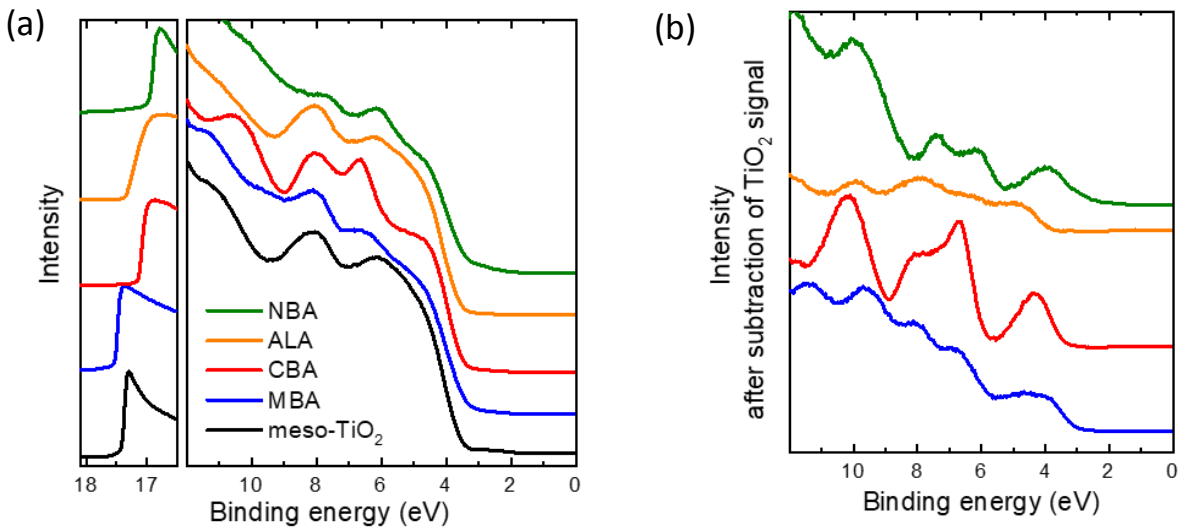

Figure 2 (a) UPS spectra of bare TiO_2 and SAMs modified TiO_2 (hν= 21.22 eV). (b) Same UPS spectra of the HOMO region after subtracting the signal originating from TiO_2 in order to identify the DOS originating from the SAM layers.

Table 1. Energy level values extracted from the UPS measurements (**Figure 2**), IPES measurements (**Figure S2**, Supporting Information), and XPS measurements (**Figure 3b**). Note that the values of VB_{TiO2}, CB_{TiO2}, $E_{B, TiO2}$, and $E_{HOMO,SAM}$ are given with respect to E_F.

Compound	$\mu_\perp$ [a] (D)	*Wf* (eV)	VB_{TiO2} (eV)	$E_{HOMO, SAM}$ (eV)	CB_{TiO2} (eV)	IE / EA (eV)	$E_{B, TiO2}$ (eV)
meso-TiO_2	0	3.8	3.57		0.15 eV	7.37 / 3.65	459.09
MBA	-0.50	3.69		3.44		7.13 / --	459.07
NBA	2.22	4.27		2.37		6.64 / --	458.89
CBA	0.89	4.08		3.00		7.08 / --	459.09
ALA	0.12	3.88		3.94		7.82 / --	459.13

[a] From Ref.[5]

The data obtained by UPS shows that the SAMs introduce significant changes in surface *Wf*, lowering its energy by ~ 110 meV for MBA and increasing it for the other SAMs, with a maximum shift of ~ 470 meV for NBA. This effect of *Wf* change can be correlated with the normal component of the dipole moments ($\mu_\perp$) of the various SAMs, which have been calculated using density functional theory (DFT) analysis. This parameter varied from -0.50 D (MBA) to 2.22 D (NBA).[5] The work function change can be expressed by the Poisson's equation:

$$Wf = \frac{N_S \mu_\perp}{\varepsilon_r \varepsilon_0} \qquad (1)$$

where N_s is the surface dipole density, ε_r is the dielectric constant and ε_0 is the permittivity of free space.

Please cite this paper as : T. Zhu, S. Olthof, Th. Pauporté, Titanium dioxide Surface Energy Levels Tuning by Self-Assembled Monolayers. Appl. Phys. Lett. 121 (2022) 141602. DOI: 10.1063/5.0107202

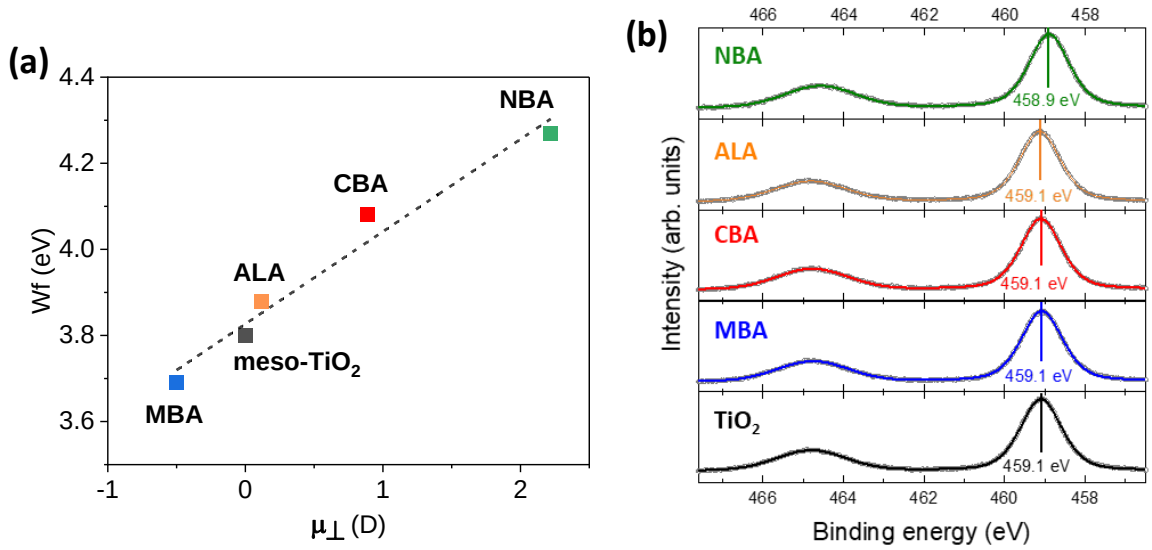

Figure 3. (a) UPS-derived work function *Wf* of the different SAMs adsorbed onto TiO_2 plotted against the calculated normal dipole moment $\mu_\perp$. (b) XPS core level signals of Ti 2p. The data (open circles) is fitted by two Voight profiles (colored line) corresponding to the $2p_{1/2}$ and $2p_{3/2}$ Signal. The position of the latter one is indicated in the graph and listed in Table 1 as $E_{B,\ TiO2}$.

To verify this trend, **Figure 3a** shows the change in measured surface *Wf* as a function of calculated $\mu_\perp$ value and confirms, within the uncertainty of the measurements, a linear relationship. The slope obtained by fitting is about 0.21 eV/D. The total change in *Wf* is around 0.58 eV, which is rather large and therefore provides a convenient way to adjust the energy level alignment at such an interface and thereby the charge carriers transferred into devices. Intriguingly, we observed that this shift in vacuum level is not a mere step in the local vacuum level due to the electric field across the SAM layer, but that to some degree also the electronic structure of the underlying TiO_2 is affected by the SAM's dipole. This is an indication for a charge transfer at the surface which was observed in additional XPS measurements of the Ti 2p core level signals. As can be seen in **Figure 3b**, MBA, CBA, and ALA SAMs do not significantly alter the Ti core level positions at the surface. However, we found that the modification by NBA, which has the strongest dipole moment, leads to a significant shift by ~ 200 meV towards lower binding energy. If there is a shift in the core level energy levels of TiO_2, then the valence band levels can be expected to do the same.[36] This approximation, as well as the other data from Table 1, are used to draw an energy level diagram of the surfaces treated with the different SAMs in **Figure 4**. We can note that for NBA, the total *Wf* shifts extracted from **Figure 2a** is divided into a contribution corresponding to shifted surface energy levels of TiO_2, as determined from the change in core level position shown in **Figure 3b**, and a step in the local vacuum level. For all other samples, the change in TiO_2 core level is negligible. It can be seen, that the meso-TiO_2 is strongly n-type which is well-known from other UPS studies and makes this material a good electron extraction layer.[37] The MBA SAM caused a vacuum level down-shift due to its negative dipole

moment while ALA, CBA, and NBA SAMs caused a vacuum level up-shift due to their positive dipole moments.

We then correlated these changes in work function with the performance of test devices containing a wide bandgap p-type organic semiconductor, Spiro-OMeTAD, and a gold anode, as previously published by us for application in UV detectors.[5]. The short circuit current (J_{sc}) and open circuit voltage (V_{oc}) generated under UV-light illumination (λ = 365 nm) are given in **Table S1** (Supporting Information). Remarkably, the J_{sc} parameter clearly scales with the dipole moment in the order of MBA < ALA < control < CBA < NBA. Here, the highest *Jsc* of 1.51 mA/cm^2 is found for NBA with its positive interface dipole shift of +0.47 eV, while MBA, which showed the negative dipole shift of -0.11 eV is unfavorable for the extraction of photogenerated electrons (J_{sc} = 0.75 mA/cm^2). This clearly indicates that charge extraction can be facilitated or hindered by this energy step and a high *Wf* SAM is advantageous for high J_{sc}. On the other hand, for the open circuit voltage, the observed order was the reversed, meaning that higher surface *Wf* led to a lowering of V_{oc} in the order of ALA > MBA > control > CBA > NBA. This can be explained by a reduction in quasi Fermi level splitting within the organic layer when the Fermi level is shifted within the band gap towards the HOMO due to the change in *Wf* by the underlying SAM.[5,38] Therefore, J_{sc} and V_{oc} cannot be optimized simultaneously and the choice must be guided by the final operating mode.

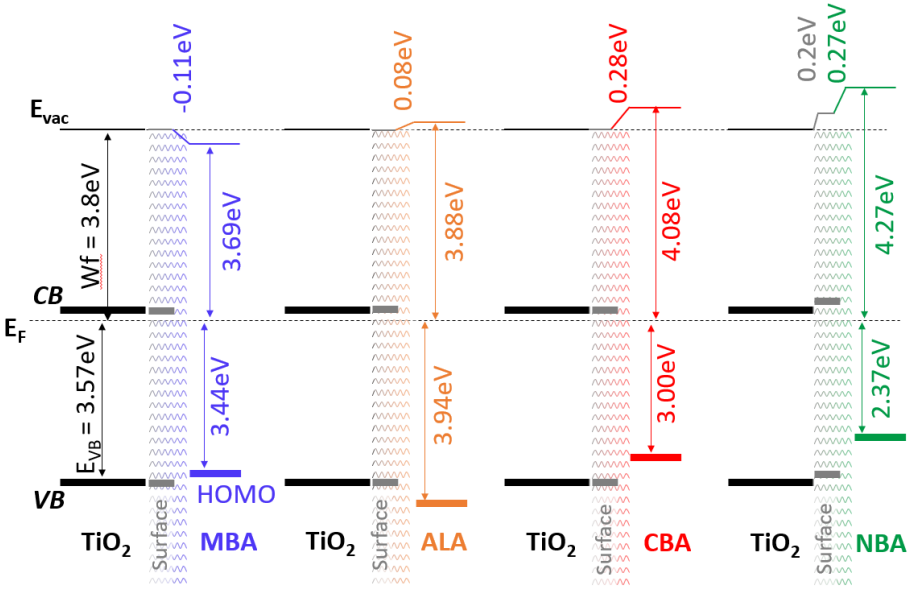

Figure 4. Energy level alignment of the different SAMs/TiO_2 systems, sketched using the data extracted from the UPS, IPES, and XPS measurements. The shaded area labeled *surface* indicates changes taking place due to the application of the SAM layer, *i.e.* changes in in TiO_2 energy levels (grey labels) as well as step in the local vacuum level position (colored labels).

In summary, we have described a step-by-step method to construct the energy band diagrams of SAM/TiO_2 systems by combining the measurements of three different photoelectron spectroscopy techniques. Our experiments show that steps in the local vacuum level, *i.e.* interface dipoles, are

introduced by the SAMs and that the resulting total changes in *Wf* correlate with the dipole moment of the SAMs. These *Wf* changes range from -0.11 eV to +0.47 eV, relative to the pure TiO_2 layer, and directly affect the J_{sc} and V_{oc} values of simple organic-inorganic hybrid test devices. The present analysis technique can be applied to other oxide/SAMs systems. Our results draw a clear picture of how the dipole moment of a SAM affects an interface and can thereby influence charge extraction and and built-in potential in optoelectronic devices.

Supplementary Material

Experimental section; FE-SEM of pristine and treated mesoporous TiO_2 layer; UPS and IPES spectra of TiO_2; Effect of SAMs on J_{sc} and V_{oc} of a photodetector.

Acknowledgements

T.Z acknowledge the CSC-Paristech program for scholarship funding (grant N° 201706340053), T.P acknowledge the Erasmus+ Agence for "Training Mobilities between Programme Countries" grant.

References

[1] J. Krüger, U. Bach, M. Grätzel, Modification of TiO_2 heterojunctions with benzoic acid derivatives in hybrid molecular solid-state devices, Adv. Mater. **12**, 447–451(2000).

[2] R. Qiao, L. Zuo, Self-assembly monolayers boosting organic–inorganic halide perovskite solar cell performance, J. Mater. Res. **33**, 387–400 (2018).

[3] E.M.J. Johansson, R. Schölin, H. Siegbahn, A. Hagfeldt, H. Rensmo, Energy level alignment in TiO_2/dipole-molecule/P3HT interfaces, Chem. Phys. Lett **515**, 146–150 (2011).

[4] K.-G. Lim, S. Ahn, T.-W. Lee, Energy level alignment of dipolar interface layer in organic and hybrid perovskite solar cells, J. Mater. Chem. C **6**, 2915–2924 (2018).

[5] T. Zhu, J. Su, J. Alvarez, G. Lefèvre, F. Labat, I. Ciofini, T. Pauporté, Response enhancement of self-powered visible-blind UV photodetectors by nanostructured heterointerface engineering, Adv. Funct. Mater. **29,** 1903981(2019).

[6] Y. Ogomi, A. Morita, S. Tsukamoto, T. Saitho, Q. Shen, T. Toyoda, K. Yoshino, S.S. Pandey, T. Ma, S. Hayase, All-solid perovskite solar cells with HOCO-R-NH_3^+ I^- anchor-group inserted between porous titania and perovskite, J. Phys. Chem. C **118**, 16651–16659 (2014).

[7] B. Li, Y. Chen, Z. Liang, D. Gao, W. Huang, Interfacial engineering by using self-assembled monolayer in mesoporous perovskite solar cell, RSC Adv. **5,** 94290–94295 (2015).

[8] L. Liu, A. Mei, T. Liu, P. Jiang, Y. Sheng, L. Zhang, H. Han, Fully Printable Mesoscopic Perovskite Solar Cells with Organic Silane Self-Assembled Monolayer, J. Am. Chem. Soc. **137**, 1790–1793 (2015).

[9] Ç. Kırbıyık, D. Akın Kara, K. Kara, S. Büyükçelebi, M.Z. Yiğit, M. Can, M. Kuş, Improving the performance of inverted polymer solar cells through modification of compact TiO_2 layer by different boronic acid functionalized self-assembled monolayers, Appl. Surf. Sci. **479** 177–184 (2019).

[10] T.N. Van, Y.K. Lee, J. Lee, J.Y. Park, Tuning hydrophobicity of TiO_2 Layers with silanization and self-assembled nanopatterning, Langmuir **29**, 3054–3060 (2013).

[11] S. Wooh, T.-Y. Kim, D. Song, Y.-G. Lee, T.K. Lee, V.W. Bergmann, S.A.L. Weber, J. Bisquert, Y.S. Kang, K. Char, Surface modification of TiO_2 photoanodes with fluorinated self-assembled monolayers for highly efficient dye-sensitized solar cells, ACS Appl. Mater. Interfaces **7,** 25741–25747 (2015).

[12] H. Bai, T. Shen, J. Tian, An air-stable ultraviolet photodetector based on mesoporous TiO_2/spiro-OMeTAD, J. Mater. Chem. C **5,** 10543–10548 (2017).

[13] T. Zhu, J. Su, F. Labat, I. Ciofini, T. Pauporté, Interfacial Engineering through Chloride-Functionalized Self-Assembled Monolayers for High-Performance Perovskite Solar Cells. ACS Appl. Mater. Interfaces **12**, 744–752 (2020).

[14] J. Cao, J. Yin, S. Yuan, Y. Zhao, J. Li, N. Zheng, Thiols as interfacial modifiers to enhance the performance and stability of perovskite solar cells, Nanoscale **7,** 9443–9447 (2015).

[15] H.B. Kim, I. Im, Y. Yoon, S. Do Sung, E. Kim, J. Kim, W.I. Lee, Enhancement of photovoltaic properties of $CH_3NH_3PbBr_3$ heterojunction solar cells by modifying mesoporous TiO_2 surfaces with carboxyl groups, J. Mater. Chem. A **3**, 9264–9270 (2015).

[16] L. Zuo, Q. Chen, N.D. Marco, Y.-T. Hsieh, H. Chen, P. Sun, S.-Y. Chang, H. Zhao, S. Dong, Y. Yang, Tailoring the interfacial chemical interaction for high efficiency perovskite solar cells, Nano Lett. **17,** 269–275 (2017).

[17] L. Zuo, Z. Gu, T. Ye, W. Fu, G. Wu, H. Li, H. Chen, Enhanced photovoltaic performance of $CH_3NH_3PbI_3$ Perovskite Solar Cells through interfacial engineering using self-assembling monolayer, J. Am. Chem. Soc. **137**, 2674–2679 (2015).

[18] A. Al-Ashouri, E. Köhnen, B. Li, A. Magomedov, H. Hempel, P. Caprioglio, J.A. Márquez, A.B. Morales Vilches, E. Kasparavicius, J.A. Smith, N. Phung, D. Menzel, M. Grischek, L. Kegelmann, D. Skroblin, C. Gollwitzer, T. Malinauskas, M. Jošt, G. Matič, B. Rech, R. Schlatmann, M. Topič, L. Korte, A. Abate, B. Stannowski, D. Neher, M. Stolterfoht, T. Unold, V. Getautis, S. Albrecht, Monolithic perovskite/silicon tandem solar cell with >29% efficiency by enhanced hole extraction, Science **370**, 1300–1309 (2020).

[19] Q. Wang, C.-C. Chueh, T. Zhao, J. Cheng, M. Eslamian, W.C.H. Choy, A.K.-Y. Jen, Effects of self-assembled monolayer modification of nickel oxide nanoparticles layer on the performance and application of inverted perovskite solar cells, ChemSusChem **10**, 3794–3803 (2017).

[20] R. Azmi, W.T. Hadmojo, S. Sinaga, C.-L. Lee, S.C. Yoon, I.H. Jung, S.-Y. Jang, High-efficiency low-temperature ZnO based perovskite solar cells based on highly polar, nonwetting self-assembled molecular layers, Adv. Energy Mater. **8**, 1701683 (2018).

[21] S. Jun, T. Zhu, T. Pauporté, I. Ciofini, F. Labat, Improving the heterointerface in hybrid organic–inorganic perovskite solar cells by surface engineering: Insights from periodic hybrid density functional theory calculations, J. Comput. Chem. **41**, 1740–1747 (2020).

[22] V. De Renzi, R. Rousseau, D. Marchetto, R. Biagi, S. Scandolo, and U. del Pennino, Metal Work-Function Changes Induced by Organic Adsorbates: A Combined Experimental and Theoretical Study, Phys. Rev. Lett. **95**, 046804 (2005).

[23] C. Schmidt, A. Witt, G. Witte, Tailoring the Cu(100) Work Function by Substituted Benzenethiolate Self-Assembled Monolayers, J. Phys. Chem. A **115**, 7234–7241 (2011).

[24] J.F. Lu, X.F. Lin,b X.C Jiao, T. Gengenbach, A.D. Scully, L. Jiang, B. Tan, J.S. Sun, B. Li, N. Pai, U. Bach, A.N. Simonov, Y.-B. Cheng, Interfacial benzenethiol modification facilitates charge transfer and improves stability of cm-sized metal halide perovskite solar cells with up to 20% efficiency, Energy Environ. Sci. **11**, 1880–1889 (2018).

[25] P. Caprioglio, D. Saul Cruz, S. Caicedo-Dávila, F. Zu, A. Adrian Sutanto, F. Peña-Camargo, L. Kegelmann, D. Meggiolaro, L. Gregori, C. M. Wolff, B. Stiller, L. Perdigón-Toro, H. Köbler, B. Li et al., Bi-functional Interfaces by Poly-Ionic Liquid Treatment in Efficient pin and nip Perovskite Solar Cells, Energy Environ. Sci. **8,** 4508-4522 (2021).

[26] J. Schnadt, J.N. O'Shea, L. Patthey, J. Schiessling, J. Krempaský, M. Shi, N. Mårtensson, P.A. Brühwiler, Structural study of adsorption of isonicotinic acid and related molecules on rutile TiO_2(110) II: XPS, Surf. Sci. **544**, 74–86 (2003).

[27] J. Schnadt, A. Henningsson, M.P. Andersson, P.G. Karlsson, P. Uvdal, H. Siegbahn, P.A. Brühwiler, A. Sandell, Adsorption and charge-transfer study of Bi-isonicotinic acid on in situ-grown anatase TiO_2 nanoparticles, J. Phys. Chem. B **108**, 3114–3122 (2004).

[28] T.L. Bahers, T. Pauporté, F. Labat, G. Lefèvre, I. Ciofini, Acetylacetone, an interesting anchoring group for ZnO-based organic−inorganic hybrid materials: a combined experimental and theoretical study, Langmuir **27**, 3442–3450 (2011).

[29] Q. Guo, I. Cocks, E.M. Williams, The adsorption of benzoic acid on a TiO_2(110) surface studied using STM, ESDIAD and LEED. Surf. Sci. **393,** 1–11 (1997).

[30] F. Blobner, P. N. Abufager, R. Han, J. Bauer, D. A. Duncan, R. J. Maurer, K. Reuter, P. Feulner, and F. Allegretti, Thiolate-Bonded Self-Assembled Monolayers on Ni(111): Bonding Strength, Structure, and Stability, J. Phys. Chem. C **119**, 15455−15468 (2015).

[31] R. Han, F. Blobner, J. Bauer, D. A. Duncan,‡ J. V. Barth, P. Feulner and F. Allegretti, Toward interfacing organic semiconductors with ferromagnetic transition metal substrates: enhanced stability via carboxylate anchoring, Chem. Commun. **52**, 9805-9808 (2016)

[32] W. Busayaporn, D. A. Duncan, F. Allegretti, A. Wander, M. Bech, P. J. Møller, B. P. Doyle, N. M. Harrison, G. Thornton, and R. Lindsay, Structure of a Model Dye/Titania Interface: Geometry of Benzoate on Rutile-TiO_2 (110)(1 × 1), J. Phys. Chem. C **120**, 14690−14698 (2016).

[33] D. I. Sayago, M. Polcik, R. Lindsay, R. L. Toomes, J. T. Hoeft, M. Kittel, D. P. Woodruff, Structure Determination of Formic Acid Reaction Products on TiO_2(110), J. Phys. Chem. B **108**, 14316-14323 (2004).

[34] P. Wang, Z. Shao, M. Ulfa, T. Pauporté, Insights into the Hole Blocking Layer Effect on the Perovskite Solar Cell Performance and Impedance Response, J. Phys. Chem. C **121**, 9131–9141(2017).

[35] M. Ulfa, P. Wang, Z. Shao, B. Viana, Th. Pauporté, Oxide Hole Blocking Selective Contacts in Perovskite Solar Cells. Proc. SPIE **10533,** 105332R (2018).

[36] S. Olthof, W. Tress, R. Meerheim, B. Lüssem, K. Leo, Photoelectron Spectroscopy Study of Systematically Varied Doping Concentrations in an Organic Semiconductor Layer Using a Molecular P-Dopant, J. Appl. Phys. **106**, 103711(2009).

[37] G. Man, J. Schwartz, J. C. Sturm, A. Kahn, Electronically Passivated Hole-Blocking Titanium Dioxide/Silicon Heterojunction for Hybrid Silicon Photovoltaics, Adv Mater. Interfaces **3**, 1600026 (2016).

[38] W. Tress, K. Leo, M. Riede, Influence of Hole-Transport Layers and Donor Materials on Open-Circuit Voltage and Shape of I-V Curves of Organic Solar Cells, Adv. Funct. Mater. **21**, 2140–2149(2011).